Mon. Not. R. Astron. Soc. **000**, 000–000 (0000) Printed 8 April 2013 (MN LaTeX style file v2.2)

arXiv:1304.1570v1 [astro-ph.GA] 4 Apr 2013

Molecular Cloud Evolution V. Cloud Destruction by Stellar Feedback

Pedro Colín[1], * Enrique Vázquez-Semadeni [1], and Gilberto C. Gómez[1]
[1] *Centro de Radiostronomía y Astrofísica, UNAM, Apartado Postal 72-3 (Xangari), 58089 Morelia, Mexico*

8 April 2013

ABSTRACT

We present a numerical study of the evolution of molecular clouds, from their formation by converging flows in the warm ISM, to their destruction by the ionizing feedback of the massive stars they form. We improve with respect to our previous simulations by including a different stellar-particle formation algorithm, which allows them to have masses corresponding to single stars rather than to small clusters, and with a mass distribution following a near-Salpeter stellar IMF. We thus refer to the stellar particles as "stars". We also employ a simplified radiative-transfer algorithm that allows the stars to feed back on the medium at a rate which depends on their mass and the local density. Our results are as follows: a) As in previous studies, the clouds formed begin to gravitationally contract long (several Myr) before star formation begins, but in turn, star formation begins several Myr before the largest scales terminate their collapse. b) Contrary to the results from our previous study, where all stellar particles injected energy at a rate corresponding to a star of $\sim 10\ M_{\odot}$, the dense gas is now completely evacuated from 10-pc regions around the stars within 10–20 Myr, suggesting that this feat is accomplished essentially by the most massive stars. c) To further test this suggestion, we performed two additional simulations where the IMF "saturates" at 8 and 20 $M_{\odot}$. In the former, the clouds are never dispersed, while in the latter they are, although over a larger timescale than in the case with a full IMF. d) At the scale of the whole numerical simulations, the dense gas mass is reduced by up to an order of magnitude, although star formation (SF) never shuts off completely, indicating that the feedback terminates SF locally, but triggers new SF events elesewhere, over distance scales of a few tens of pc. e) The SF efficiency (SFE) is maintained at the $\sim 10\%$ level, depending on the geometry, even though the gas continues to always infall onto the local star forming regions. We speculate that the inclusion of supernova explosions and magnetic fields should bring the SFE down to the few-percent level.

Key words: interstellar matter – stars: formation – turbulence

1 INTRODUCTION

Understanding how star formation (SF) proceeds in our Galaxy, and other galaxies in general, is a key quest in astrophysics. In recent years, it has become clear that the evolution and distribution of SF in the Galaxy is intimately linked to the structure and evolution of the molecular clouds (MCs) where it takes place (see, e.g., the reviews by Mac Low & Klessen 2004; Ballesteros-Paredes et al. 2007; McKee & Ostriker 2007; Vázquez-Semadeni 2013, and references therein).

In a series of previous papers (Vázquez-Semadeni et al. 2006, 2007, 2010, 2011), we have investigated, alongside other groups (Hennebelle & Pérault 1999, 2000; Audit & Hennebelle 2005; Hennebelle & Audit 2007; Audit & Hennebelle 2010; Hennebelle et al. 2008; Heitsch et al. 2005; Heitsch et al 2006; Heitsch & Hartmann 2008; Heitsch et al. 2009; Banerjee et al. 2009), the evolution of MCs and of their SF activity, from their formation by condensation of the atomic gas in the interstellar medium to their star-forming stages and, in some studies, to their destruction by stellar feedback (Vázquez-Semadeni et al. 2010). Among the above studies, those including self-gravity (Vázquez-Semadeni et al. 2007, 2010, 2011; Heitsch & Hartmann 2008; Heitsch et al. 2009) have shown that the coherent formation of large clouds (several tens of parsecs) leads to the onset of global gravitational contraction throughout the cloud, at a stage when the cloud is still mostly composed of atomic hydrogen, with

---

* e-mail: p.colin@crya.unam.mx

© 0000 RAS

SF only starting several Myr later, when the cloud has become mostly molecular.

This result, however, is in contradiction with the largely established notion that MCs cannot be collapsing freely, since otherwise their resulting SF rates (SFRs) would be up to two orders of magnitude larger than observed (Zuckerman & Palmer 1974). A related property is that the observed SF efficiency (SFE, the fraction of a cloud's mass that ends up in stars) for whole giant molecular clouds (GMCs) is estimated to be of only a few percent (e.g. Myers et al. 1986). Hence, it is generally believed that MCs must be in or near equilibrium, supported against their self-gravity by supersonic turbulence, magnetic fields, or some combination thereof. Specifically, a number of SF theories have appeared in recent years in which the underlying scenario is that MCs are supported globally by turbulent pressure, while gravitational collapses occur only locally, caused by the supersonic turbulent compressions (e.g., Padoan & Nordlund 2002, 2011; Krumholz & McKee 2005; Hennebelle & Chabrier 2011, see also the discussion by Federrath & Klessen 2013).

Of course, an alternative explanation has been known for over four decades (e.g., Field 1970; Whitworth 1979; Elmegreen 1983; Cox 1983; Franco, Shore & Tenorio-Tagle 1994) for the low observed SFE of GMCs, namely that stellar feedback, mainly from the ionizing radiation from massive stars, may disrupt the clouds before they have converted much of their mass into stars. In this scenario, there is no need to support the clouds against their self-gravity. Also, this scenario becomes even more feasible in view of the recent result, from numerical simulations of cloud formation and evolution, that the collapsing clouds undergo *hierarchical gravitational fragmentation* (Vázquez-Semadeni et al. 2009). That is, the turbulent density fluctuations, having larger mean densities than that of the whole parent GMC, have shorter free-fall times and smaller Jeans masses, and therefore the densest clumps begin to form stars earlier than the rest of the cloud, and before the global collapse of the cloud terminates.

In Vázquez-Semadeni et al. (2010, hereafter Paper I), we carried out a first attempt to numerically capture this phenomenology, by performing simulations of cloud formation and evolution in the presence of ionization heating from massive stars, which is considered to be the main feedback mechanism affecting GMCs of masses up to $\sim 10^5~M_\odot$ (Matzner 2002; Krumholz & Matzner 2009; Dale et al. 2012). In Paper I, the instantaneous, time-dependent SFE was defined as

$$\mathrm{SFE}(t) = \frac{M_*(t)}{M_{\mathrm{dense}}(t) + M_*(t)}, \tag{1}$$

where M_{dense} is the mass in dense gas ($n > 100~\mathrm{cm}^{-3}$) and M_* is the total mass in stars. It was found in that paper that the prescription for ionization-heating feedback used there was able to maintain the SFE at the few-percent level throughout the evolution of the cloud, while control simulations not including it reached SFEs roughly an order of magnitude larger. Also, an analytical model representing this scenario was recently presented by Zamora-Avilés et al. (2012), and shown to correctly describe several evolutionary properties of GMCs and their SF activity.

However, one shortcoming of the feedback prescription used in Paper I was that it assumed that the stars responsible for the feedback all injected energy into the medium at a rate roughly corresponding to that of a $\sim 10~M_\odot$ star. This implied that the stellar feedback was possibly overestimated for clouds forming low-mass stars, and underestimated for clouds forming high-mass stars. In particular, Paper I found that the GMC-like clouds could not be destroyed by the feedback. Instead, Dale et al. (2012), for example, have been able to disrupt clouds up to $10^6~M_\odot$ by means of ionization feedback. In Paper I, the SFE was kept low because the conversion of dense gas into stars was locally inhibited by the feedback, but not because the clouds at large were destroyed. Only the local clumps were destroyed.

In the present paper, we improve on the numerical prescription used in Paper I in two ways. First, we use a probabilistic SF prescription instead of a fully deterministic one. As it turns out, this probabilistic prescription allows us to produce a mass spectrum for stellar particles, which can be tuned to resemble the Salpeter initial mass function (IMF). Second, once armed with a realistic stellar mass spectrum, we incorporate a mass-dependent ionization heating prescription for the feedback from the stellar particles produced in the simulations, applying a simplified description of radiative transfer, neglected in Paper I. We expect that, with this prescription, we can obtain a more realistic description of the effect of ionization feedback on MCs of various masses.

The plan of the paper is as follows. In Sec. 2, we describe the numerical model, focusing in particular in the heating and cooling functions employed (Sec. 2.2), the stellar-particle formation prescription (Sec. 2.3), the feedback prescription (Sec. 2.4), and the refinement criterion used (Sec. 2.1). We next describe the details and parameters of the simulations in Sec. 3, and then present our results in Sec. 4. In Sec. 5 we compare our results with those of Paper I and discuss some of their implications. Finally, in Sec. 6 we present a summary and some conclusions.

2 THE NUMERICAL MODEL

The numerical simulations used in this work were performed using the adaptive mesh refinement (AMR) + N-body Adaptive Refinement Tree code ART (Kravtsov et al. 1997, 2003). In the following sections we describe the adaptations we have performed to it for application to our problem of interest.

2.1 Refinement

The numerical box is initially covered by a grid of 128^3 (zeroth level) cells. The mesh is subsequently refined as the matter distribution evolves. The maximum allowed refinement level was set to five, so that high-density regions have an effective resolution of 4096^3 cells, with a minimum cell size of 0.0625 pc. As in Paper I, cells are refined when the gas mass within the cell is greater than $0.32 M_\odot$. That is, the cell size is refined by a factor of 2 when the density increases by a factor of 8, so that, while refinement is active, the grid cell size Δx scales with density n as $\Delta x \propto n^{-1/3}$. Once the maximum refinement level is reached, no further refinement is performed, and the cell's mass can reach much larger values.

Note that this constant-cell-mass refinement criterion does not conform to the so-called *Jeans criterion* (Truelove et al. 1997) of resolving the Jeans length with at least 4 grid cells. Truelove et al. (1997) cautioned that failure to do this might result in spurious, numerical fragmentation. However, we do not consider this a cause for concern since, as will be described in Sec. 2.3, our star formation prescription allows us to choose the stellar-particle mass distribution, and tune it to a Salpeter (1955) value.

2.2 Heating and cooling

The main additional physical processes implemented in our simulations, and relevant to the physical problem studied here are a) the cooling and heating of the gas; b) its conversion into stars; c) the stellar feedback via ionization-like heating, and d) the self-gravity from gas and stars.

We use heating (Γ) and cooling (Λ) functions of the form

$$\begin{aligned} \Gamma &= 2.0\times10^{-26}\ \mathrm{erg\ s^{-1}} \qquad (2)\\ \frac{\Lambda(T)}{\Gamma} &= 10^{7}\exp\left(\frac{-1.184\times10^{5}}{T+1000}\right)\\ &+\ 1.4\times10^{-2}\sqrt{T}\exp\left(\frac{-92}{T}\right)\ \mathrm{cm}^{3}. \qquad (3) \end{aligned}$$

These functions are fits to the various heating and cooling processes considered by Koyama & Inutsuka (2000), as given by equation (4) of Koyama & Inutsuka (2002). As noted in Vázquez-Semadeni et al. (2007), eq. (4) in Koyama & Inutsuka (2002) contains two typographical errors. The form used here incorporates the necesary corrections, kindly provided by H. Koyama (2007, private communication). With these heating and cooling functions, the gas is thermally unstable in the density range $1 \lesssim n \lesssim 10\ \mathrm{cm}^{-3}$.

2.3 Star formation prescription: a probabilistic approach

In our simulations, SF is modeled as taking place in the densest regions, defined by $n > n_{\mathrm{SF}}$, where n is the gas density, and n_{SF} is a density threshold. If a grid cell meets this density criterion, then a stellar particle (SP) of mass m_* may be placed in the cell, with probability P, every timestep of the coarsest grid. If the SP *is* created, it acquires half of the mass of its parent cell, and this mass is removed from the cell. Thereafter, the particle is treated as non-collisional and follows N-body dynamics. No other criteria are imposed. We set $n_{\mathrm{SF}} = 9.2\times10^{4}\ \mathrm{cm}^{-3}$, which corresponds to a cell mass of 0.78 $M_\odot$ at the highest refinement level. This fixes the minimum value for SP masses at 0.39 $M_\odot$. Note that, as in Paper I, our SPs differ from the commonly-used sink particles (Bate et al. 1995; Federrath et al. 2010), mainly in that our SPs are not allowed to accrete after they form. Thus, we refrain from calling them as "sinks", and use the nomenclature "stellar particles" instead. However, as we describe below, our probabilistic approach to SP formation allows us to obtain a realistic mass distribution (IMF) for them.

A few items are worth noting about our SF prescription. First, note that, once the maximum refinement level is reached, no further refinement is applied to a cell (cf. Sec. 2.1) even if its density keeps increasing. Moreover, since the creation of an SP is a probabilistic event, the density of a cell where a gravitational collapse is going on continues to increase until an SP forms in the cell. Some authors have advocated the prescription that, once the maximum refinement level has been reached, a sink particle is created at the cell density that would correspond to the next refinement level (e.g., Federrath et al. 2010) in order to always fulfill the Jeans criterion and thus completely avoid spurious fragmentation (Truelove et al. 1997) until the sink particles are formed. However, we forgo of this recommendation since, as will be seen in what follows, our prescription allows us to *impose* the desired IMF of the SPs, and thus artificial fragmentation is not a concern.

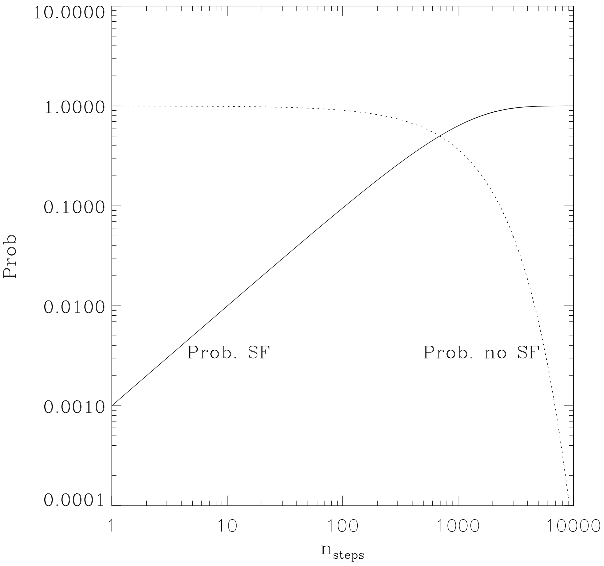

Figure 1. Probability of having (*solid line*) and *not* having formed (*dashed line*) a stellar particle (SP) in a cell that meets the density criterion $n > n_{\mathrm{SF}}$ after a certain number of coarse-grid time steps for $P = 0.001$.

The prescription we use implies that the longer it takes to form an SP in a collapsing cell, the more massive the SP will be, because the cell's density will be higher. The probability of *not* having formed an SP after n_{steps} time steps is $\mathcal{P}_{\mathrm{no}} = (1-P)^{n_{\mathrm{steps}}}$, while the probability of having formed it is $\mathcal{P}_{\mathrm{yes}} = 1-(1-P)^{n_{\mathrm{steps}}}$. These probabilities are shown in Fig. 1 for $P = 0.001$. Serendipitously, we have found that the resulting mass distribution of the SPs is a power law, with an exponent that depends on the value of P. Thus, P is a control parameter that allows us to generate a stellar mass spectrum with the desired slope. In Figure 2 we show the evolution of the stellar mass spectrum in simulation LAF1$_{5l}$ (cf. Sec. 3) with $P = 0.003$. The slope of the function changes from -1.21 at $t = 25.6$ Myr to -1.34 at the end of the evolution, thus hovering close to the Salpeter value of -1.35. The most massive SP formed in this simulation has $m_* = 61\ M_\odot$, while the least massive ones have masses $m_* \sim 0.5\ M_\odot$. Note that we have no turnover of the IMF at small masses, but this is inconsequential for our purposes, since we are only interested in the feedback exerted by the stars on their parent cloud, and the low-mass stars exert no

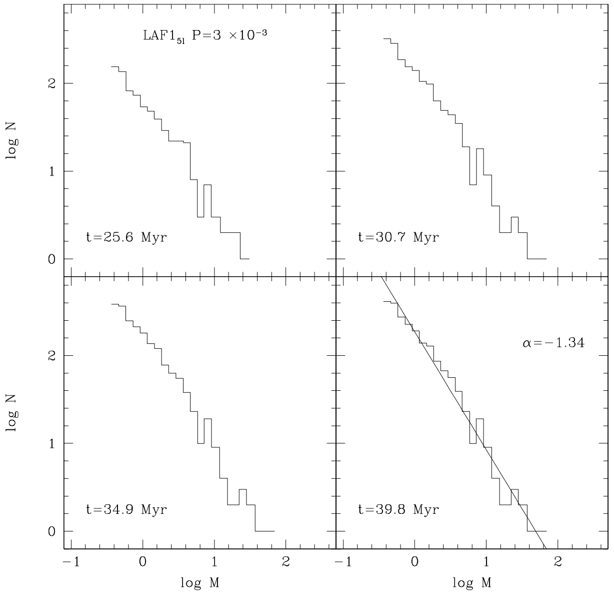

Figure 2. Evolution of the spectrum of stellar masses for simulation LAF1$_{5l}$. The spectrum at any epoch can be well fitted by a power law. In the lower right panel, with a line, we also show this fit and the value of its slope.

significant feedback at the GMC scale (see, e.g., the review by Vázquez-Semadeni 2011, and references therein)

Finally, we note that, because now the SPs form in cells whose density is typically much larger than the threshold value $n_{\rm SF}$, in the present paper we choose $n_{\rm SF} = 9.2 \times 10^4$ cm^{-3}, to allow for a sufficiently large number of SPs to form. This is significantly smaller than the value used in Paper I, where SPs formed always at a density very similar to $n_{\rm SF}$. Moreover, we stress that, contrary to the situation in our previous papers, our SPs now have masses corresponding to individual stars rather than to small clusters, and so, in what follows, we shall indistinctly refer to them simply as "stars".

2.4 Feedback prescription

Another important difference of our new feedback prescription, compared to that in Paper I, is in the way we implement the ionization feedback by massive stars. In Paper I, SPs injected thermal energy only to the cell where they were located (hereafter, the "stellar cell"), at a rate high enough to produce a realistic HII region[1]. Instead, here we now model the birth and evolution of HII regions by assigning a temperature of 10^4 K to all cells whose distance d to the SP satisfies the condition

$$d < R_{\rm s} \equiv \left(\frac{3}{4\pi}\frac{S_*}{\alpha n_{\rm LOS}^2}\right)^{1/3}, \tag{4}$$

where $R_{\rm s}$ is the Strömgren (1939) radius, S_* is the flux of ionizing photons produced by the star, $\alpha = 3.0 \times 10^{-13}$ cm^3 s^{-1} is the recombination coefficient, and $n_{\rm LOS}$ is a characteristic particle number density along the line of sight between the stellar cell and the test cell, which we discuss below. If it turns out that $R_{\rm s}$ is smaller than the size of the stellar cell, we simply set the temperature of this cell equal to 10^4 K, and no further calculation is done. On the other hand, if $R_{\rm s}$ is larger than the stellar cell's size, then it is necessary to determine whether $d < R_{\rm s}$ or not. In principle, this poses a radiative transfer problem since, as is well known, eq. (4) is valid only for the case when the medium between the stellar and the test cells has a uniform density. However, if the medium is not uniform, then the photoionization-recombination balance must be computed along the line joining the SP and the grid cell in question (see, e.g., Dale et al. 2007), a procedure that can be quite computationally expensive.

As a zeroth-order approximation to solve this problem, we opt for choosing a value for $n_{\rm LOS}$ that can be deemed representative of the typical density along the path from the SP to the grid cell. Specifically, we take the geometric mean of the densities at these two locations in the simulation, $n_{\rm LOS} = \sqrt{n_{\rm SP}\ n_{\rm test}}$. This approximation for $R_{\rm s}$ is, of course, crude, and will miss, for example, shadowing effects due to intervening dense clumps between the stellar and the test cells but, for the purpose of modeling the large-scale dynamics of the MC containing these cells, we consider it is sufficient. We jokingly refer to this scheme as a "poor man's radiative transfer" (PMRT) scheme.

For the ionizing flux S_*, which depends on the SP's mass, we use the tabulated data provided by Díaz-Miller et al. (1998). Note that only SPs with a mass greater than 1.9 $M_\odot$ inject any significant ionizing feedback into the ISM, implying that only the massive SPs influence the dynamics of the molecular clouds. Finally, note that we turn off the cooling for the cells whose temperature is set to 10^4 K. Otherwise, very dense cells would radiate away their thermal energy very quickly. Their temperature is held at 10^4 K for a time $t_{\rm s}$, which we assume depends on the star's mass m_* as

$$t_{\rm s} = \begin{cases} 2\ \text{Myr} & \text{if } m_* \le 8M_\odot; \\ 222\ \text{Myr}\ \left(\frac{m_*}{M_\odot}\right)^{-0.95} & \text{if } m_* > 8M_\odot. \end{cases} \tag{5}$$

For stars more massive than $8M_\odot$, this time is a fit to the stellar lifetimes by Bressan etal. (1993), while for stars with masses lower than that, it represents the fact that the duration of the stellar-wind phase is ∼ 2 Myr, roughly independently of mass. This also means that we are representing the effect of the winds and outflows of low mass stars by an ionization prescription. While this is clearly only an approximation, we do not expect it to have much impact on our calculations, since the main source of feedback energy at the level of GMCs is the ionization feedback from massive stars (Matzner 2002).

Our prescription for the ionization feedback for massive stars was tested by running simulations of a box of 32 pc on a side, without self-gravity, filled with gas at uniform temperature and density, of 42 K and 100 cm^{-3}, respectively. These simulations used a resolution of 256^3 cells, with the adaptive refinement switched off. A massive SP ($m_* = 27\ M_\odot$) was placed in the center of the box, and the system was allowed to evolve freely. Figure 3 shows the expansion of the resulting HII region, which is comprised of those cells with tem-

---

[1] Because the thermal energy was dumped only in the cell were the SP was formed, neighboring cells were heated by numerical conduction.

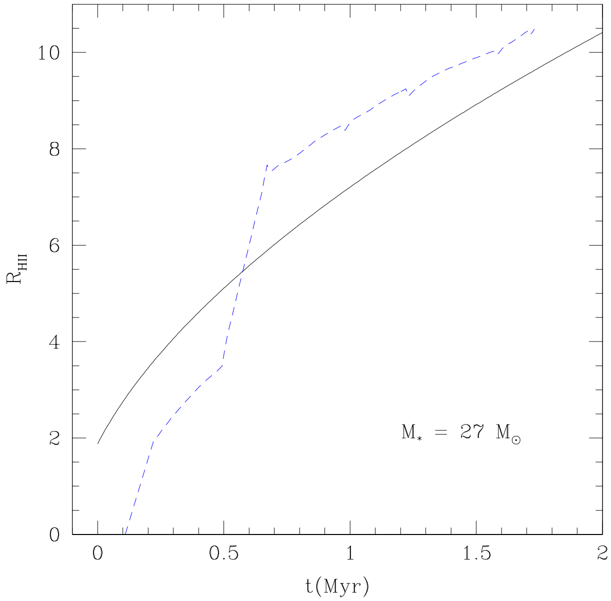

Figure 3. Evolution of the HII region produced by a 27-$M_\odot$ star in a box of 32 pc per side. The black solid line represents the analytic solution given by eq. (6), while the blue dashed line is the radius of the HII region in the simulation. Temperatures of target cells located inside the Strömgren sphere, centered on the SP, are set to 10^4 K. The cooling is switched off in these cells during the lifetime of the star.

peratures greater than a few thousand degrees. Also shown in this figure is the well known analytical solution (Spitzer 1978),

$$R_s(t) = R_i \left(1 + \frac{7}{4}\frac{c_s t}{R_i}\right)^{4/7}, \tag{6}$$

where R_i is the initial Strömgren radius and c_s is the sound speed. The numerical solution is seen to agree with the analytic one to within $\sim 30\%$, an accuracy we consider sufficient, given our interest only in the large-scale evolution of the clouds.

3 THE SIMULATIONS

Our simulations use the same initial setup as the runs in Paper I, which represents the evolution of a region of 256 pc per side, initially filled with warm gas at a uniform density of $n_0 = 1$ cm^{-3} and a temperature $T_0 = 5000$ K, implying an adiabatic sound speed $c_{\rm s} = 7.4$ km s^{-1} (assuming a mean particle mass $\mu = 1.27$). The full numerical box thus contains $5.25 \times 10^5 M_\odot$. In this medium, we make two streams collide with a speed $v_{\rm inf} = 5.9$ km s^{-1} each (corresponding to a Mach number of 0.8 with respect to the unperturbed medium) along the x-direction (see Figure 1 of Vázquez-Semadeni et al. 2007). The streams have a radius of 64 pc and a length of 112 pc each, so that the total mass in the two inflows is $9.0 \times 10^4 M_\odot$. Note that the streams are completely contained within the box, so that the compression they produce is a single event. There is no continuous flow through the boundaries, as we use periodic boundary conditions.

On top of the inflow velocity we superpose a field of initial low-amplitude turbulent velocity fluctuations, in order to trigger the instabilities in the compressed layer that will cause it to fragment and become turbulent (Heitsch et al. 2005; Vázquez-Semadeni et al. 2006). As in Paper I, we create this initial velocity fluctuation field with a new version of the spectral code used in Vázquez-Semadeni et al. (1995) and Passot et al. (1995), modified to run in parallel in shared-memory architectures. The simulations are evolved for about 40 Myr.

The collision nonlinearly triggers a transition to the cold phase, forming a turbulent, cold, dense cloud (Hennebelle & Pérault 1999; Audit & Hennebelle 2005; Heitsch et al. 2005; Heitsch et al 2006; Vázquez-Semadeni et al. 2006), consisting of a complex network of sheets, filaments, and clumps of cold gas embedded in a warm diffuse substrate (Audit & Hennebelle 2005; Hennebelle & Inutsuka 2006; Hennebelle & Audit 2007). The complex as a whole quickly engages in gravitational collapse (Vázquez-Semadeni et al. 2007). Moreover, the local density fluctuations become unstable and collapse in a shorter time than the global time because they are embedded in a contracting medium and thus have shorter collapse times (Toalá et al. 2013). Eventually, they proceed to forming stars, which then heat their environment, forming expanding "HII regions" that tend to disperse the clouds.

Although our results are based essentially on two simulations, a few more runs were performed with a twofold purpose: to compare the old prescription for feedback to the new one, and to assert the importance of the most massive SPs in the disruption of the clouds. All simulations but one were run using the "large-amplitude" (LA) initial velocity fluctuations ($v_{\rm rms} \sim 1.7$ km s^{-1}) as opposed to the "small-amplitude" (SA) case ($v_{\rm rms} \sim 0.1$ km s^{-1}) (see Paper I). Clearly, more fragmentation and more complex cloud structures are expected in the LA runs, thus causing them to produce somewhat smaller clouds that resemble low- or intermediate-mass star-forming clouds. On the other hand, the SA run allows us to consider a case of very high coherence and uniformity, which tends to form a high-mass star-forming region (Vázquez-Semadeni et al. 2009), and furthermore resembles the conditions we used in previous papers (Vázquez-Semadeni et al. 2007, 2011).

The nomenclature for the runs introduced in Table 1 continues to use the acronyms LAF or SAF used in Paper I, where F stands for feedback. A number 1 or 0 after the letter F means feedback is on or off, respectively. The test simulations are denoted with "old", 8 or 20 after the word LAF.

4 RESULTS

4.1 LAF1 and SAF1 runs

The new schemes for the probabilistic star formation recipe and for the ionization feedback by massive stars were used to run the SAF1 and LAF1 simulations. Figures 4 and 5 show, for the full simulated box, the evolution of the mass in dense gas ($n > 100$ cm^{-3}), the mass in stars, the mass in both components, and the star formation rate (SFR) and efficiency (SFE), in the SAF1 and LAF1 runs, respectively.

Table 1. Parameters of the Simulations

Run name	$v_{\rm rms}$ [km s^{-1}]	Feedback
SAF1	0.1	New prescription, full IMF
LAF1	1.7	New prescription, full IMF
LAF0	1.7	Off
LAFold	1.7	Old prescription from Paper I
LAF8	1.7	New prescription, max stellar mass = 8 $M_\odot$
LAF20	1.7	New prescription, max stellar mass = 20 $M_\odot$

In contrast to Paper I, we now define the instantaneous SFE as

$$\mathrm{SFE}(t) = \frac{M_*(t)}{M_{\rm max}(t) + M_*(t)}, \tag{7}$$

where $M_{\rm max}$ is the maximum mass in dense gas reached between the start of the simulation and time t. This is because in the present simulations the clouds are eventually dispersed, and thus the SFE evaluated with the instantaneous dense gas mass approaches unity at late stages of evolution, but not because all the dense gas has been converted to stars, but rather because the remaining gas is evaporated by the stars. Our definition gives us instead an approximate measure of the net SFE, that is, the fraction of the dense gas mass ever present in a given volume and over a certain time interval that is converted into stars.

In both runs, the evolution of the mass in dense gas is similar (see the top left panels of Figs. 4 and 5): first, dense gas starts to accumulate as the evolution proceeds until it reaches a maximum, then the effect of the radiation feedback is such that it overcomes the buildup of dense gas by gravitacional accretion. Also, in both runs, SPs continue to form after the maximum in the mass in dense gas is reached, albeit at a significantly declining rate. Later in the evolution, in the LAF1 run, the mass in dense gas begins to increase again. This time the density does not reach the threshold for star formation and thus no new SPs are formed (see bottom left panels of Figs. 4 and 5).

In run SAF1, the largest star-forming region forms in the center of the box, due to the coherent collapse of the entire sheet-like cloud formed by the collision. As in Paper I, we refer to this region as "the Central Cloud". We enclose the cloud in a cylinder of radius 10 pc and length 20 pc located at the center of the box. Figure 6 shows the evolution of the mass in dense gas, the SFE, the mass in stars, and the SFR for the Central Cloud. This figure is similar to Fig. 4 (or Fig. 5) except that the bottom right panel now shows the evolution of the SFR instead of the evolution of the total mass. Unlike what happens with the whole box, where some dense gas still remains by the end of the evolution, here we witness the complete dispersal of the cloud from this region. In addition, in the lower left panel we see that the mass in SPs also decreases by the end of the evolution. Because our SPs have no winds and do not explode as supernovae, this can can only mean that the stellar cluster, formed from the dense gas mass of the cloud, is being dispersed as well (that is, its constituent stars are leaving the cylinder that initially contained the cloud).

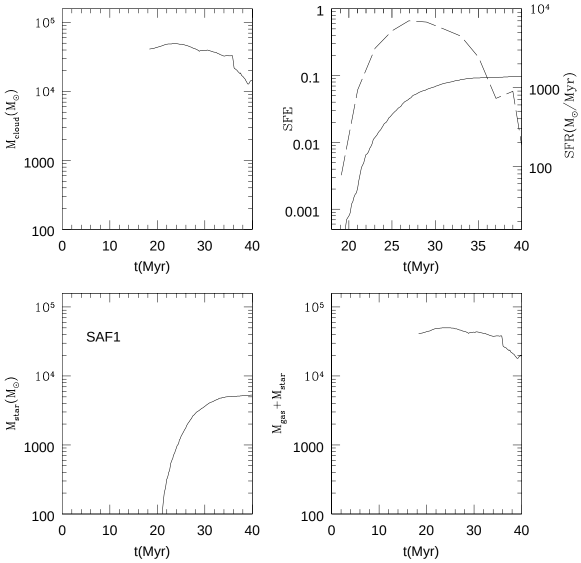

Figure 4. Evolution of the mass in dense gas (top left panel), the star formation rate (SFR; dashed line) and efficiency (SFE; solid line) (top right panel), the mass in SPs (bottom left panel), and the total mass (stars plus dense gas, bottom right panel) in the whole box in run SAF1. As a result of the destruction of the dense gas the mass in SPs as well as the SFE reaches a maximum before the end of the evolution.

In the case of run LAF1, the clouds identified as Cloud 1 and Cloud 2 in Paper I are also used here to study the cloud evolution and star formation activity. Again, cylinders of the same size as that used with the Central Cloud are placed around Clouds 1 and 2. As in Fig. 6, Figs. 7 and 8 also show the evolution of the mass in dense gas, the SFE, the mass in stars, and the SFR for Cloud 1 and Cloud 2, respectively. As with the Central Cloud in run SAF1, Cloud 1 is also destroyed, and no stars are left inside the cylinder where the cloud initially was; that is, the stellar cluster associated with the cloud is dispersed, in ∼ 12 Myr. Cloud 2 is also completely destroyed, but unlike Cloud 1, here we still can find SPs inside its corresponding cylinder, as it was the case for the Central Cloud. Figure 9 shows the evolution in the neighborhood of Cloud 2 over 15 Myr, illustrating these results.

4.2 Feedback scheme comparison

In the feedback scheme of Paper I, HII regions were created by the injection of thermal energy from SPs. The energy was deposited entirely in the cell where the stars were lo-

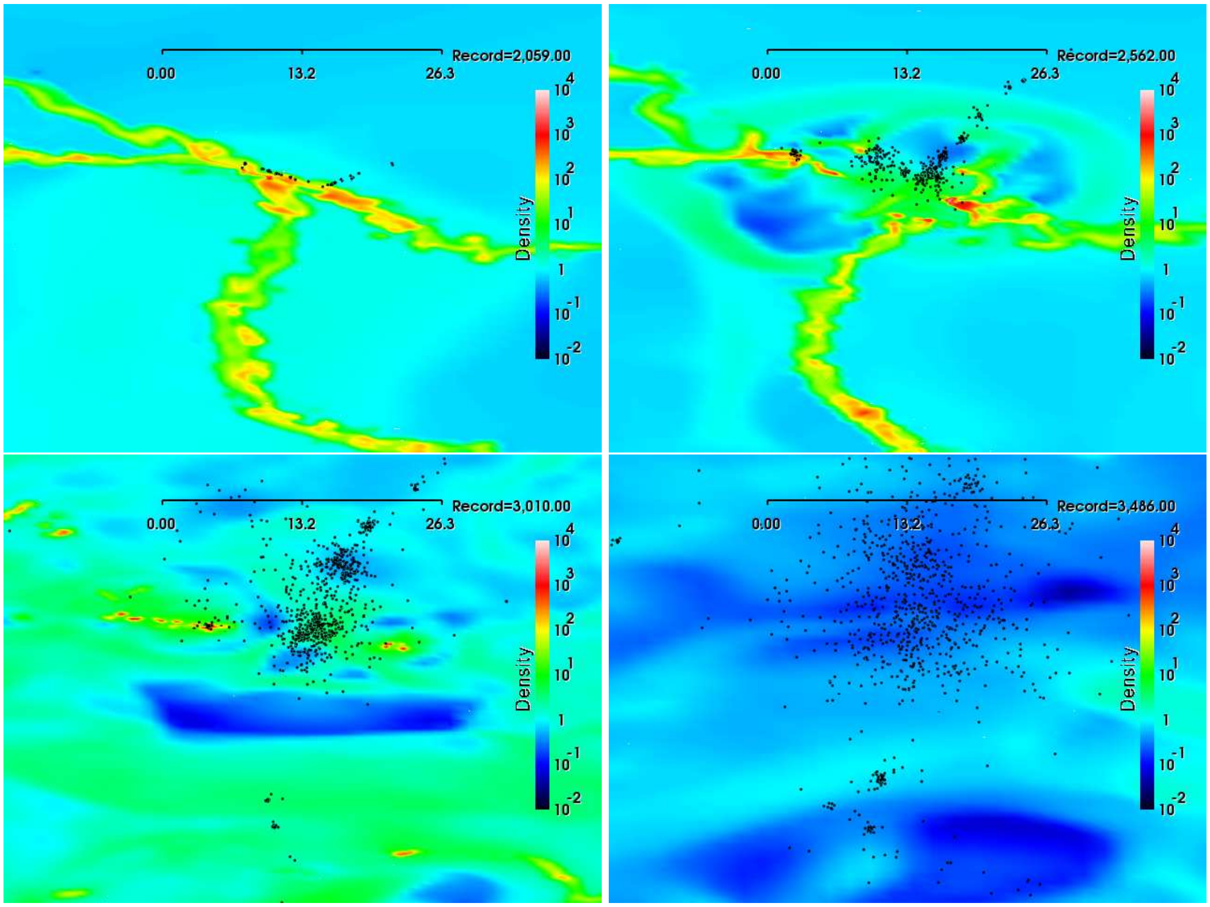

Figure 9. Cross-section images of the density field in the neighborhood of Cloud 2 in run LAF1, at times (in Myr) 20.59 (top left), 25.62 (top right), 30.1 (bottom left), and 34.86 (bottom right), showing the dispersal of the cloud. The black dots show the stellar particles (SPs). The horizontal ruler shows a scale of 26.3 pc. Note that the density field is shown on an inclined cross section through the simulation, but the SPs are shown in 3D space, so all particles in front to the density plane can be seen. Note the complete dispersal of the cloud within 15 Myr.

cated, and thus neighboring cells were heated exclusively by conduction, rather than by radiative heating. The value of the rate at which the energy was dumped was chosen so as to produce reasonably realistic HII regions. Additionally, the cooling in the heated cell was turned off, since otherwise most of energy would be radiated away in these initially very dense cells. Thus, it is not feasible to directly compare the results of our new simulations, with the PMRT scheme used in the present paper. However, it is important to compare the old prescription with the new one used in the present paper in a controlled manner, to assess the differences induced by the prescription, in addition to the differences induced by the presence of a stellar IMF. Therefore, we have run another LAF-type simulation, labeled LAFold, which uses the old feedback prescription from Paper I, and in which all SPs with $M_* > 10\ M_\odot$ inject thermal energy at a rate equal to that used in Paper I.

Figure 10 shows the evolution of the mass in dense gas, the SFE, the stellar mass, and the total (dense gas plus stars) mass for runs LAF1 (black solid lines), LAF0 (red dotted lines) and LAFold (blue, short-dashed lines), together with two other runs to be discussed in the next section (see Table 1). We see that the LAFold run does not disrupt the clouds, in line with the results of Paper I.

4.3 The role of the most massive stars in the destruction of the clouds

To assert the importance of the feedback of the massive stars in the destruction of the clouds, two extra LAF models were run, labeled LAF8 and LAF20. LAF8 (magenta long-dashed lines in Fig. 10) is a run with the new feedback prescription, but with all SPs with $M_* > 10\ M_\odot$ ionizing their surroundings *as if they were a star of* 8 $M_\odot$. LAF20 (cyan dot-dashed lines), moreover, is a run similar to LAF1 but in this case the feedback “saturates” at 20 $M_\odot$; that is, all SPs with $M_* < 20\ M_\odot$ have the feedback they should according to their mass, but those SPs with $M_* \geq 20\ M_\odot$ exert a feedback as if they were a star of 20 $M_\odot$.

From Fig. 10 we see that, like run LAFold, run LAF8 does not destroy the clouds; the mass in dense gas in the whole simulated box (and in the individual clouds, not shown) continues to increase. Run LAF20 is an intermediate case between those runs in which clouds are not destroyed and run LAF1: in run LAF20, the mass in dense gas reaches a peak before the end of the evolution. Because the feedback in run LAF20 is not as strong as it is in run LAF1, this maximun is reached few Myr later. This experiment demostrates

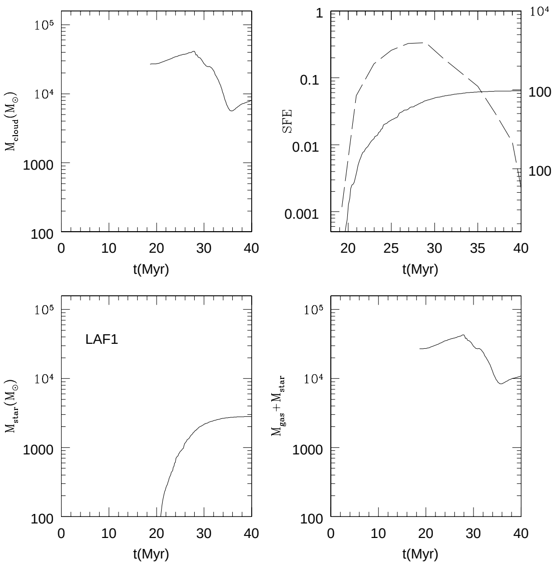

[htb!]

Figure 5. Evolution of the mass in dense gas (top left panel), the SFR (dashed line) and SFE (solid line; top right panel), the mass in SPs (bottom left panel), and the total mass (stars plus dense gas, bottom right panel) in the whole box for run LAF1. Unlike the SA run, here the star formation does not stop abruptly, and instead a slow decline in the star formation rate is observed.

that stars with $M_* \geq 20\ M_\odot$ are crucial for the destruction of clouds of masses up to a few times $10^4\ M_\odot$.

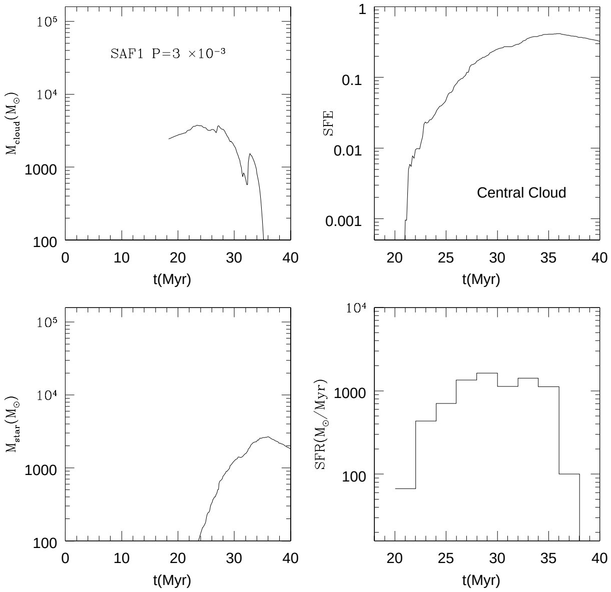

Figure 6. Evolution of the mass in dense gas (top left panel), the SFE (top right panel), the mass in SPs (bottom left panel), and the SFR (bottom right panel) in the Central Cloud in run SAF1. Ioinization feedback is so efficient that the cloud only lives abut 10 Myr. Interestingly, the stellar cluster is almost dispersed in the next 10 Myr of evolution.

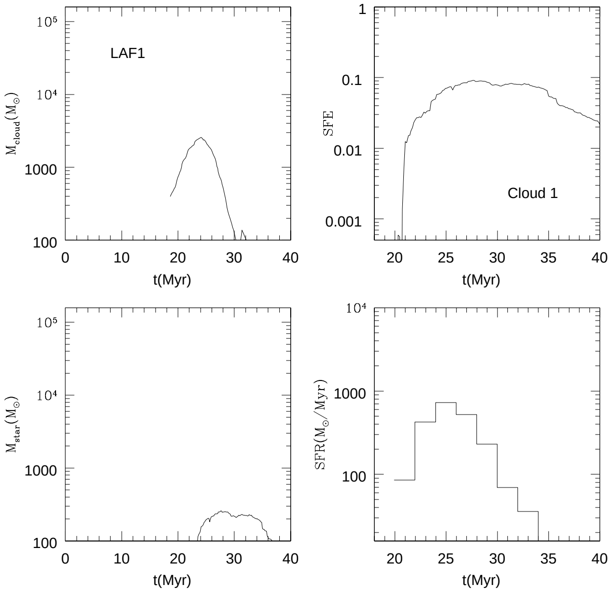

Figure 7. Evolution of the mass in dense gas (top left panel), the SFE (top right panel), the mass in SPs (bottom left panel), and the SFR (bottom right panel) in Cloud 1 of run LAF1.

5 DISCUSSION

5.1 Comparison with previous work

The effect of feedback has been studied by numerous workers, both analytically and numerically (see, e.g., the review by Vázquez-Semadeni 2011, and references therein). In particular, the pioneering numerical simulations of Bania & Lyon (1980) included various cases of heating and cooling functions for the medium, and used radiative transfer (on a 40 × 40 two-dimensional grid) to include the effects of photoionization from OB stars in a 180-pc square region, making them a direct precursor of this work. Even at their very limited resolution, they foresaw several outcomes of this setup, such as the formation and maintenance of a cloud population, that the clouds would be gravitationally unstable had self-gravity been included, and that the SFR would be self-consistent if 0.1–0.5 of the mass in the clouds were to go into the formation of new massive stars, thus making a prediction for the SFE. However, their required SFE for self-consistency was too high, presumably because self-gravity was not included in their simulations. This limitation also meant that the feedback stars had to be placed randomly in the simulation. Subsequent numerical works focused mostly on the effect of supernova feedback on the structuring of the ISM on kiloparsec scales (e.g., Rosen et al. 1993; Rosen & Bregman 1995; de Avillez 2000; Mac Low et al. 2005; Joung & Mac Low 2006; Wood et al. 2010; Hill et al. 2012) but, in general, self-gravity has not been included in these works, and the supernova rate has been an input parameter for the simulations, rather than a self-consistent output.

Another line of study has been the simulation of feedback by stellar outflows at the clump (parsec) scale, aiming at either maintenance of the turbulence within the clumps (e.g., Li & Nakamura 2006; Carroll et al. 2009; Cunningham et al. 2009), or at the self-regulation of star formation (e.g., Li & Nakamura 2006; Nakamura & Li 2007; Wang et al. 2010). The latter are closest in aim to our

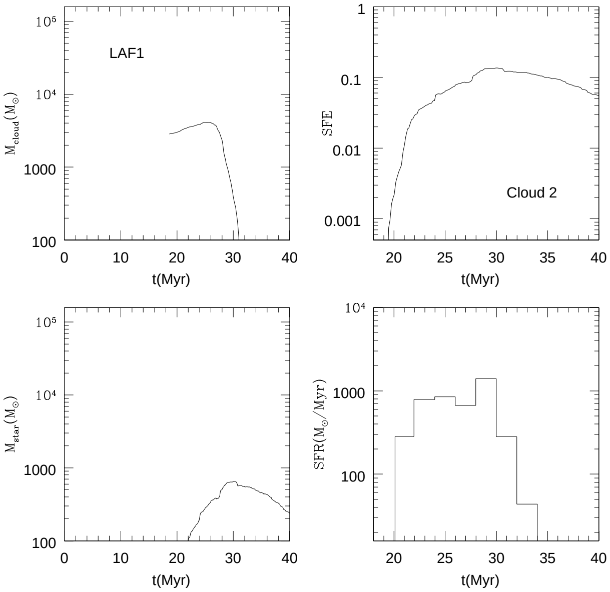

Figure 8. Evolution of the mass in dense gas (top left panel), the SFE (top right panel), the mass in SPs (bottom left panel), and the SFR (bottom right panel) in Cloud 2 of run LAF1.

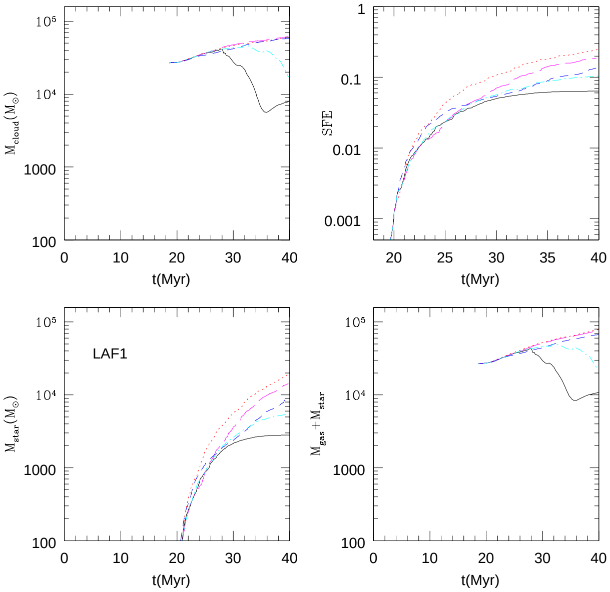

Figure 10. Evolution of the mass in dense gas (top left panel), the SFE (top right panel), the mass in SPs (bottom left panel), and the total mass (stars plus dense gas, bottom right panel) in the whole numerical box of each of the five LAF runs in the whole box: run LAF1 (black solid lines); run LAF0, with no feedback (red dotted lines); run LAFold (blue short-dashed lines), with the feedback prescription from Paper I; run LAF8 (magenta long-dashed lines), with the new feedback prescription but with all SPs with $M_* > 10\ M_{\odot}$ ionizing their surroundings as if they had a mass of 8 $M_{\odot}$; and finally, run LAF20 (cyan dot-dashed lines), in which all SPs with $M_* < 20\ M_{\odot}$ feed back according to their masses, but SPs with $M_* \geq 20\ M_{\odot}$ feed back as if they were a star of 20 $M_{\odot}$.

present study, although not in scale, as they only consider parsec-sized regions, and only outflow feedback, which corresponds to the effect of low- and intermediate-mass stars, which does not seem to be the dominant driver at the GMC scale (Matzner 2002).

Our results in this paper are most directly comparable to those of Dale et al. (2012), who performed a parameter-space study of the disruptive effect of photoionizing radiation of molecular clouds of various masses. Thus, the basic physical processes at play in their simulations are very similar to those included in ours. Their main result is that, while clouds of masses up to $\sim 10^5\ M_{\odot}$ can be readily destroyed by the ionization feedback from their newly-formed stars, clouds with $M \sim 10^6\ M_{\odot}$ cannot be destroyed, as their escape velocities are larger than the sound speed in the photoionized gas. This regime is not sampled by our simulations, in which the total dense gas mass is never more massive than a few times $10^4\ M_{\odot}$.

The main differences between our setup and theirs are that they use a polytropic equation of state covering only a temperature range corresponding to molecular and cold atomic gas, and that they start with a suite of initial clouds in various configurations, while we let the clouds form self-consistently out of the warm ISM. Also, they include the photoionized gas resulting from the stellar feedback, but their simulations lack the warm (neutral and ionized) substrate in which the clouds dwell, and out of which they form in our simulations. That is, in their simulations there is no possibility of the warm environment penetrating into the clouds, as proposed theoretically by Hennebelle & Inutsuka (2006), and suggested observationally by Krčo et al. (2008). Thus, our self-consistently formed clouds may be more porous, and thus less bound, than those of Dale et al. (2012). Also, our probabilistic SF prescription allows our SPs to be individual stars always and with a realistic IMF. This means that our simulations can be employed for future cluster dynamics studies. Instead, the sinks in the simulations by Dale et al. (2012) have a mass range that goes from individual stars to small clusters. Moreover, they only considered the effect of stars more massive than 20 $M_{\odot}$, so they did not investigate the effect of stars of different masses. On the other hand, their radiative transfer algorithm is more realistic than ours, and they sample a larger parameter space. Thus, in general, it can be said that the two studies are highly complementary in nature, each one providing a different perspective of the problem: specifically, they focused on the ability of photoinizing radiation to destroy clouds of different masses, while we have focused on the control of the SFE and the role of stars of different masses and different feedback prescriptions.

Most importantly, our simulations are relevant in the context of studying the entire evolutionary cycle of molecular clouds, and showing that star-forming GMCs as a whole can be in a global state of gravitational contraction, which is initiated during their pre-molecular stages, and yet comply with the low observed SFR and SFE in The Galaxy, as a consequence of the stellar feedback, but not by maintaining them hovering around an equilibrium state (Krumholz et al 2006; Goldbaum et al. 2011), but rather by photoevaporating them while the collapse motions continue.

5.2 Limitations

Our simulations, although one step ahead of our previous effort from Paper I, are still far from being all-inclusive. Most notably, we have neglected supernova explosions and magnetic fields, and moreover, our radiative transfer scheme is very rudimentary. We plan to improve on these issues in future work. Here we can speculate what should be the effect of these processes on our results.

From Sec. 4.1, we see that the SFE (measured with respect to the maximum dense gas mass) in our simulations, shown in Figs. 4–8, with only one exception (Fig. 7), is larger than $\sim 5\%$, and reaches 30% in the case of the Central Cloud (Fig. 6). This suggests that, in order to match the observed efficiencies of a few percent, a factor of a few percent further reduction in the SFE is still necessary. This can indeed be accomplished by magnetic fields (e.g., Vázquez-Semadeni et al. 2005; Vázquez-Semadeni et al. 2011; Nakamura & Li 2005) and/or supernova explosions, which we plan to include in future studies.

Concerning the radiative transfer (RT), our rudimentary PMRT scheme does not account for the real column density between an ionizing source and the test grid cell to be ionized, but only aims to represent it by taking the geometric mean of the density at the source and at the test cell. Thus, if a dense clump lies between these two cells, our scheme will miss it, together with any shadowing effect it may have. Thus, our scheme may tend to overestimate the photoionized volume. We do not expect this effect to be dominant, since the volume covered by shadows is not large, but comparisons should be performed once a more thorough RT algorithm is implemented.

6 SUMMARY AND CONCLUSIONS

In this paper we have presented a numerical study of the entire evolutionary cycle of molecular clouds, starting from their formation by converging flows in the warm ISM, and concluding with their dispersion by the photoinization feedback from the massive stars formed within them. Our study extended the one presented in Paper I in two main areas. First, we included a probabilistic scheme for star formation, which serendipitously allowed us to produce a stellar population following a realistic IMF, in turn allowing us to overcome a shortcoming of Paper I, namely that all stellar particles (SPs) radiated with the same intensity, roughly corresponding to that of a ~ 10–$M_\odot$ star. Second, we introduced our “poor man’s radiative transfer scheme”, PMRT, which allowed us to produce mass-dependent Strömgren spheres, and thus allowing to study the effect of stars of different masses in the dispersal of their parent clouds.

We performed numerical simulations with initial conditions identical to those used in Paper I, but varying the feedback schemes, in order to quantify the difference between our old and new feedback schemes (PMRT *versus* dumping all the energy in a single grid cell) and the effect of including stelar populations of different mass ranges. The simulation with small-amplitude initial velocity fluctuations, SAF1 (see Table 1), due to the larger coherence of the converging motions in the warm gas, leads to the formation of a single, more massive cloud at the center of the grid, which we called “The Central Cloud”. Instead, the simulations with large-amplitude initial fluctuations, generically denoted LAF, produce various less-massive clouds in the numerical box, away from the center of the simulation. From these we selected two, which we labeled Clouds 1 and 2.

We showed that cylindrical regions of length and diameter equal to 10 pc were completely evacuated of dense gas on timescales ~ 10 Myr when a full IMF was included in the calculations, and in fact, the total dense gas mass in the numerical box is reduced by a factor ~ 5 in the SAF1 simulation within ~ 20 Myr, and by a factor ~ 10 in run LAF1 within ~ 15 Myr. Instead, when the most massive stars ($M > 8\ M_\odot$) are not included in the simulations (runs LAFold and LAF8), the total dense gas mass in the simulations is hardly affected, although the SFE is reduced to levels $\sim 20\%$. When stars up to 20 $M_\odot$ are included (run LAF20), the total dense gas mass in the simulation is reduced at a level comparable to that of run LAF1, but on a timescale almost twice as long. Thus, our results strongly suggest that the destruction of the clouds is accomplished by stars with masses $M \gtrsim 20\ M_\odot$.

Our simulations also show that star formation events can be completely terminated, and the dense gas completely dispersed, on scales $\lesssim 10$ pc by the photoionizing effect of the newly formed stars in those regions, while at larger scales the dense gas contents is decreased but not completely destroyed, and the SFR is analogously decreased but not terminated. This suggests that the stellar photoionizing feedback can locally disrupt the clouds and terminate SF, but this triggers new SF events at new locations in the clouds.

Finally, our simulations show that the scenario in which large, dense and cold clouds begin to collapse even before they are mostly molecular, and continue doing so trhough their star-forming stages is perfectly consistent with the observed values of the SFE.

REFERENCES

de Avillez, M. A. 2000, *MNRAS*, 315, 479
Audit, E. & Hennebelle, P. 2005, A&A 433, 1
Audit, E., & Hennebelle, P. 2010, *A&A*, 511, A76
Ballesteros-Paredes, J., Klessen, R. S., Mac Low, M.-M., & Vázquez-Semadeni, E. 2007, Protostars and Planets V, 63
Banerjee, R., Vázquez-Semadeni, E., Hennebelle, P., & Klessen, R. S. 2009, *MNRAS*, 398, 1082
Bania, T. M., & Lyon, J. G. 1980, *ApJ*, 239, 173
Bate, M. R., Bonnell, I. A., & Price, N. M. 1995, *MNRAS*, 277, 362
Bressan, A., Fagotto, F., Bertelli, G., & Chiosi, C. 1993, A&AS, 100, 647
Carroll, J. J., Frank, A., Blackman, E. G., Cunningham, A. J., & Quillen, A. C. 2009, *ApJ*, 695, 1376
Cunningham, A. J., Frank, A., Carroll, J., Blackman, E. G., & Quillen, A. C. 2009, *ApJ*, 692, 816
Cox, D. P. 1983, *ApJ Lett.*, 265, L61
Dale, J. E., Ercolano, B., & Bonnell, I. A. 2012, *MNRAS*, 424, 377
Dale, J. E., Ercolano, B., & Clarke, C. J. 2007, *MNRAS*, 382, 1759

Diaz-Miller, R. I., Franco, J., & Shore, S. N. 1998, *ApJ*, 501, 192

Elmegreen, B. G. 1983, *MNRAS*, 203, 1011

Elmegreen, B. G., & Lada, C. J. 1977, *ApJ*, 214, 725

Federrath, C., Banerjee, R., Clark, P. C., & Klessen, R. S. 2010, *ApJ*, 713, 269

Federrath, C., & Klessen, R. S. 2013, ApJ, in press (arXiv:1209.2856)

Field, G. B. 1970, Memoires of the Societe Royale des Sciences de Liege, 19, 29

Franco, J., Shore, S. N., & Tenorio-Tagle, G. 1994, ApJ 436, 795

Goldbaum, N. J., Krumholz, M. R., Matzner, C. D., & McKee, C. F. 2011, *ApJ*, 738, 101

Goldreich, P., & Kwan, J. 1974, ApJ 189, 441

Heitsch, F., Ballesteros-Paredes, J., & Hartmann, L. 2009, *ApJ*, 704, 1735

Heitsch, F., Burkert, A., Hartmann, L., Slyz, A. D. & Devriendt, J. E. G. 2005, ApJ 633, L113

Heitsch, F., & Hartmann, L. 2008, *ApJ*, 689, 290

Heitsch, F., Slyz, A., Devriendt, J., Hartmann, L., & Burkert, A. 2006, ApJ 648, 1052

Hennebelle, P., & Audit, E. 2007, *A&A*, 465, 431

Hennebelle, P., Banerjee, R., Vázquez-Semadeni, E., Klessen, R. S., & Audit, E. 2008, *A&A*, 486, L43

Hennebelle, P., & Chabrier, G. 2011, *ApJ Lett.*, 743, L29

Hennebelle, P., & Inutsuka, S.-i. 2006, *ApJ*, 647, 404

Hennebelle, P., & Pérault, M. 1999, *A&A*, 351, 309

Hennebelle, P., & Pérault, M. 2000, *A&A*, 359, 1124

Hill, A. S., Joung, M. R., Mac Low, M.-M., et al. 2012, *ApJ*, 750, 104

Joung, M. K. R., & Mac Low, M.-M. 2006, *ApJ*, 653, 1266

Koyama, H. & Inutsuka, S.-I. 2000, ApJ 532, 980

Koyama, H. & Inutsuka, S.-I. 2002, ApJ, 564, L97

Kravtsov, A.V., Klypin, A.A., & Khokhlov, A.M., 1997, *ApJ Suppl.*, 111, 73

Kravtsov, A.V. 2003, *ApJ*(Letters), 590, 1

Krčo, M., Goldsmith, P. F., Brown, R. L., & Li, D. 2008, *ApJ*, 689, 276

Krumholz, M.R., Matzner, C.D., & McKee, C.F. 2006, ApJ, 653, 361

Krumholz, M. R., & Matzner, C. D. 2009, *ApJ*, 703, 1352

Krumholz, M. R., & McKee, C. F. 2005, *ApJ*, 630, 250

Krumholz, M. R., & Tan, J. C. 2007, *ApJ*, 654, 304

Li, Z.-Y., & Nakamura, F. 2006, *ApJ Lett.*, 640, L187

Mac Low, M.-M., Balsara, D. S., Kim, J., & de Avillez, M. A. 2005, *ApJ*, 626, 864

Mac Low, M. -M. & Klessen, R. S. 2004, Rev. Mod. Phis., 76, 125

Matzner, C. D. 2002, ApJ, 566, 302

McKee, C. F., & Ostriker, E. C. 2007, ARA&A, 45, 565

Miller, G.E., & Scalo, J.M. 1979, *ApJ Suppl.*, 41, 513

Myers, P. C., Dame, T. M., Thaddeus, P., Cohen, R. S., Silverberg, R. F., Dwek, E. & Hauser, M. G. 1986, ApJ, 301, 398

Nakamura, F., & Li, Z.-Y. 2005, *ApJ*, 631, 411

Nakamura, F., & Li, Z.-Y. 2007, *ApJ*, 662, 395

Norman, C., & Silk, J. 1980, *ApJ*, 238, 158

Padoan, P., & Nordlund, Å. 2002, *ApJ*, 576, 870

Padoan, P., & Nordlund, Å. 2011, *ApJ*, 730, 40

Passot, T., Vazquez-Semadeni, E., & Pouquet, A. 1995, *ApJ*, 455, 536

Rosen, A., & Bregman, J. N. 1995, *ApJ*, 440, 634

Rosen, A., Bregman, J. N., & Norman, M. L. 1993, *ApJ*, 413, 137

Salpeter, E. E. 1955, *ApJ*, 121, 161

Spitzer, L. 1978, Physical Processes in the Interstellar Medium (New York:Wiley)

Strömgren, B. 1939, *ApJ*, 89, 526

Toalá, J.A., Vázquez-Semadeni, E., & Góomez, G. 2012, ApJ, 744, 190

Toalá, J.A., Vázquez-Semadeni, E., Colín, P. & Góomez, G. 2013, in prep.

Truelove, J. K., Klein, R. I., McKee, C. F., Holliman, J. H., II, Howell, L. H., & Greenough, J. A. 1997, *ApJ Lett.*, 489, L179

Vázquez-Semadeni, E. 2011, Computational Star Formation, IAU Proceedings 270, 275

Vázquez-Semadeni, E. 2013, in “Magnetic Fields in Diffuse Media”, E. de Gouveia dal Pino and A. Lazarian, eds. (arXiv:1208.4132)

Vázquez-Semadeni, E., Banerjee, R., Gómez, G. C., et al. 2011, *MNRAS*, 414, 2511

Vázquez-Semadeni, E., Colín, P., Góomez, G., Ballesteros-Paredes, J., & A.W. Watson. 2010, *ApJ*, 715, 1302 (Paper I)

Vázquez-Semadeni, E., Gómez, G. C., Jappsen, A. K., Ballesteros-Paredes, J., González, R. F., & Klessen, R. S. 2007, *ApJ*, 657, 870

Vázquez-Semadeni, E., Gómez, G. C., Jappsen, A.-K., Ballesteros-Paredes, J., & Klessen, R. S. 2009, *ApJ*, 707, 1023

Vázquez-Semadeni, E., Kim, J., Shadmehri, M., & Ballesteros-Paredes, J. 2005, *ApJ*, 618, 344

Vázquez-Semadent, E., Passot, T., & Pouquet, A. 1995, *ApJ*, 441, 702

Vázquez-Semadeni, E., Ryu, D., Passot, T., González, R. F., & Gazol, A., 2006, ApJ, 643, 245

Wang, P., Li, Z.-Y., Abel, T., & Nakamura, F. 2010, *ApJ*, 709, 27

Whitworth, A. 1979, *MNRAS*, 186, 59

Wood, K., Hill, A. S., Joung, M. R., et al. 2010, *ApJ*, 721, 1397

Zamora-Avilés, M., Vázquez-Semadeni, E., & Colín, P. 2012, *ApJ*, 751, 77

Zuckerman, B., & Evans, N. J. 1974, ApJ, 192, L149

Zuckerman, B. & Palmer, P. 1974, ARA&A, 12, 279